13th Int Symp on Applications of Laser Techniques to Fluid Mechanics
Lisbon, Portugal, 26-29 June, 2006
Paper No. 1333

Measurements of Near Wall Turbulent Structure in a Microbubble Flow Using a Highly Magnifying Telecentric PIV/PTV System

Kazushi Aoki[1], Koichi Hishida[1] and Yoshiaki Kodama[2]

1: Department of System Design Engineering,Faculty of Science and Technology, Keio University,

Hiyoshi 3-14-1, Kohoku-ku, Kanagawa, Japan, mail: aoki@mh.sd.keio.ac.jp

2: National Maritime Research Institute, Shinkawa 6-38-1, Mitaka-shi, Tokyo, Japan,

Abstract An experimental investigation has been made regarding a turbulent structure of a horizontal channel flow with microbubbles. In the present study, we approached by two techniques, one is a Highly Magnifying Telecentric PIV/PTV system, and another is a measurement using a shear stress sensor. In bubbly flow, the PTV measurement is hampered by existence of a large number of bubbles in optical path and scatter light on the bubble surface. The system enables clear measurements of bubbles and liquid phase from closer distance by using rectangular prisms and telecentric lens, and bubbles' form measurements by using laser induced fluorescent and shadow imaging technique. The experiments have been carried out for flow conditions with Reynolds number ranging from 10,000 to 50,000 and void fraction up to 0.04. In the case of Reynolds number is 10,000, the large bubbles of approximately 5mm in diameter, which creep on the wall, increased a velocity gradient near the wall. The velocity profile was reduced with the increasing of the air injection by the bubble's diameter and form for Reynolds number of 30,000. In contrast, there was no noticeable change of the flow structure by bubbles for Reynolds number of 50,000, since bubbles diffused to the distant region from the wall. The shear stress measurements indicated that an increase by up to 40% of the drag force for Reynolds number is 10,000. On the other hand, the drag force was decreasing with an increasing of void fraction for Reynolds number is 30,000 to 50,000. The results of the shear stress sensor confirmed the Highly Magnifying Telecentric PIV/PTV measurements.

1. Introduction

Drag reduction techniques have been investigated to improve the transport efficiency for ships. The skin friction makes up 80% of the total drag of a large ship like a tanker, thus the reduction of the drag reduction is important for reducing fuel cost and environmental burden. There are some drag reduction devices such as riblets, polymer, LEBU and microbubble. Microbubble is an effective, easy to apply and environmentally friendly technique for reduction of local skin friction.

McCormick and Bhattacharayan (1973) detected drag reduction on an axisymmetric body by generating small bubbles by electrolysis. Madavan et al. (1984) injected air bubbles through a porous plate and showed that frictional drag reduction by microbubbles reaches 80%. Kodama et al. (2000) carried out microbubble experiments using a 50m-long flat plate model ship whose scale is close to that of a full-scale ship. The mechanism of drag reduction is mainly ascribed to the difference of mass density between gas and liquid phases. Bogdevich et al. (1977) pointed out that when bubbles distribute in banks at the surface of the object, water in the liquid phase is blocked from the surface and frictional drag is reduced. It was experimentally shown that high drag reduction corresponds to high local void fraction in the near wall region. An alternative explanation for reduction in friction drag is the 'turbulence restraint effect' where bubbles are hypothesized to reduce turbulence within the boundary layers. Kato et al. (1998), through LDV measurements in the near-wall region, suggested that the turbulent intensity is lower when drag reduction is achieved. They confirmed that turbulence intensity increases and Reynolds stress decreases with increasing void fraction. However, the mechanism for drag reduction is not yet fully understood; the

interaction between microbubbles and drag reduction at the near wall region in the turbulent bubbly flow is to be understood to achieve highly efficient drag reduction.

It is important to measure wall shear stress for estimating drag reduction effect. Several devices have been developed and used for measurement of local wall shear stress. Yoshino et al. (2004) developed a micro hot film wall shear stress sensor for feedback control of wall-turbulence, and improved its dynamic characteristics. Gür and Leehey (1989) developed a novel wall shear stress gauge to measure torque acting on a cylindrical body due to the shearing flow of the viscous sub-layer. Wang (1993) developed a wall shear stress sensor based on the difference of pressure across a porous element. However, most of these measurements need to be calibrated and have problems, for instance the microbubble penetrates into a gap on the sensor probe. Saito et al. (2004) applied an optical shear stress sensor, which enables the noncontact measurement, to the bubble channel flow, and indicated that microbubble decreases velocity gradient when it passes near the wall.

Recently, optical measurement techniques using image processing have been applied to bubbly flow. Kitagawa et al. (2005), using PIV/ LIF/ SIT, suggested that bubbles reduce Reynolds stresses in a bubble flow. However, until recently a microscopic flow structure in the vicinity of a wall has been hardly reported.

In the present study, the authors have developed a measurement system for turbulent flow structure near the wall in microbubble flow by a highly magnifying optical system using rectangular prisms and a telecentric lens. In addition, a shear stress sensor was applied to estimate of the drag reduction effect. It is the object of the study that the clarifying the mechanism of the drag reduction by the measurement of the flow structure and the measurement of the wall shear stress.

2. Experimental setup

2.1 Flow channel

Figure 1 shows a schematic diagram of experimental apparatus. It consisted of two tanks, for storage and rectification, and a two-dimensional acrylic flow channel with a cross section of 15mm × 100mm. The water as the working fluid circulated through the pump controlled by an inverter, electro magnetic flow meter, the rectification tank, test section, the storage tank. The test section is 1250mm downstream from the entrance of the flow channel and a detachable acrylic plate was mounted. We defined the center of the laser seat for visualization on the wall as the origin. The flow and width direction is defined as the x- and y- axis, respectively. Experimental conditions are listed in Table 1.

2.2 Bubble Generator

Bubble generator shown in Figure 2 was mounted at 500mm upstream from the test section. As bubble generator, we used a sintered cupper plate which nominal diameter is 2μm. The air pressure and flow rate was controlled by a pressure gauge and flow meter, respectively.

The amount of injected air is expressed by the volume ratio a defined as

$$\alpha \equiv \frac{Q_a}{Q_w + Q_a}, \qquad (1)$$

where Q_a is a volumetric flow rate of air in the test section, Q_w is a vlometric flow rate of water in the test section.

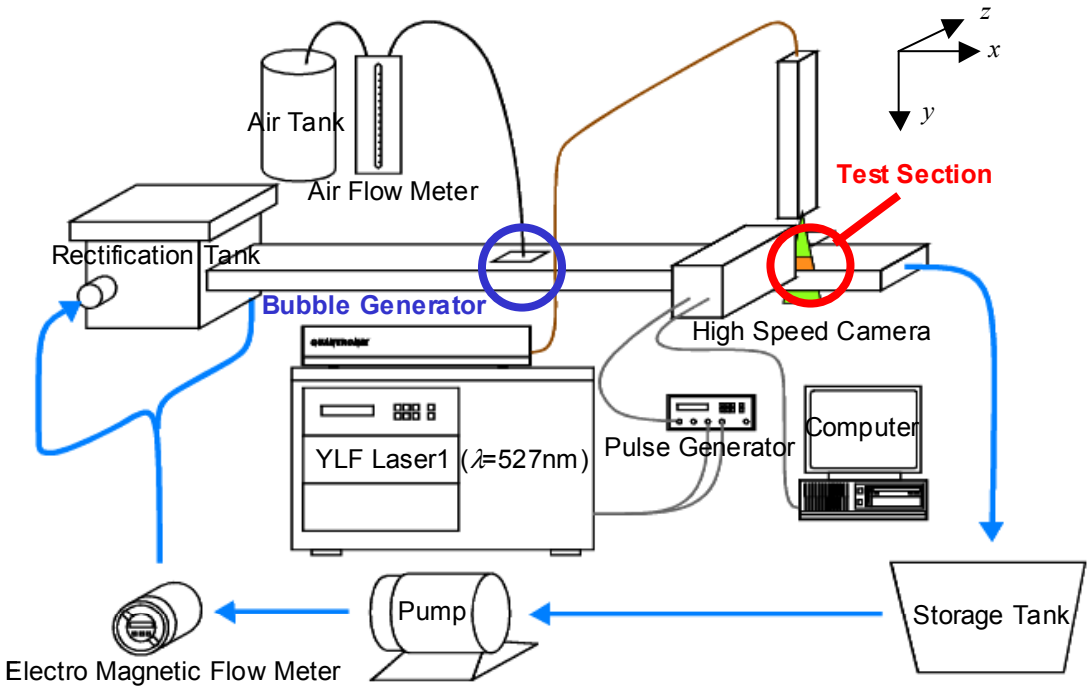

Figure 1. Schematic diagram of experimental apparatus.

Table 1. Experimental conditions.

Working fluid	Water
Channel size	1300mm × 15mm × 100mm
Channel half height	h = 7.5 [mm]
Temperature of Fluid	T = 24.0 - 25.0 [deg C]
Mean fluid velocity	U_m = 1.22 – 6.11 [m/s]
Reynolds number	Re = hU_m/ν = 10,000 - 50,000
Bulk void fraction	α = 0.01 - 0.04
Dynamic viscosity of fluid	ν = 0.91 × 10^{-6} [m^2/s]

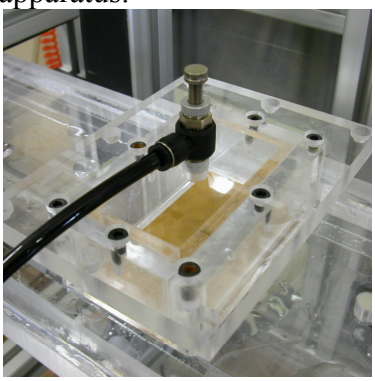

Figure 2. Schematic photograph of bubble generator.

3. Measurement system

3.1 High magnifying telecentric PIV/PTV

In a bubbly flow the PTV measurement is hampered by bubbles, because a large number of bubbles exist in the optical path. Therefore, we used a prismatic optical system to the microbubble channel flow to measure bubbles and liquid phase from a closer distance as shown in Figure 3. The optical system composed of two 15mm right angle prisms, a telecentric objective lens, a 2× tele-converter lens, and a color filter. The telecentric lens has the advantages of minimum distortion, high magnification, and contains bias brightness. For the measurements of flow structures around the bubbles, specifically to detect the interaction between bubble's motion and the flow field, we utilized a high speed PIV system. Light reflected from the bubbles saturated the CMOS device and overwhelmed the tracer particles' signal, making it difficult to detect the tracer particle images in the vicinity of the bubbles. Thus the fluorescent particles (Lefranc et Bourgeios, FLASHE Painting, mean particle diameter ≈ 10μm) were used as the tracer particles. The light source is an YLF Laser (λ=527nm, duration is less than 150nsec). We could detect fluorescence emitted by the particles in

the vicinity of the bubbles, through the color filter (565nm - 700nm : T ≥ 90%, 532nm : T ≤ 0.05%) which cut the microbubble reflections. This enabled the measurement of the liquid phase and the bubbles' form by using SIT with LEDs (λ = 607nm). The frame rate of the high-speed camera (Vision Research, Phantom V7.1) was set at 25 kHz. The image size was 256 × 128 pixels, and the CMOS pixel sheet along with the optical system corresponded to a measurement area of 2096 μm × 1048 μm. In order to capture the flow field simultaneously, the high-speed cameras and the triggering of the YLF laser were synchronized with a pulse generator.

Figure 4 depicts the example of caputured images and PTV vectors. For the preparative experiments, the bubble diameter was reduced by adding 3-pentanol. The white spot in the image corresponds to the fluorescent particle, and the PTV vectors were calculated in time series images.

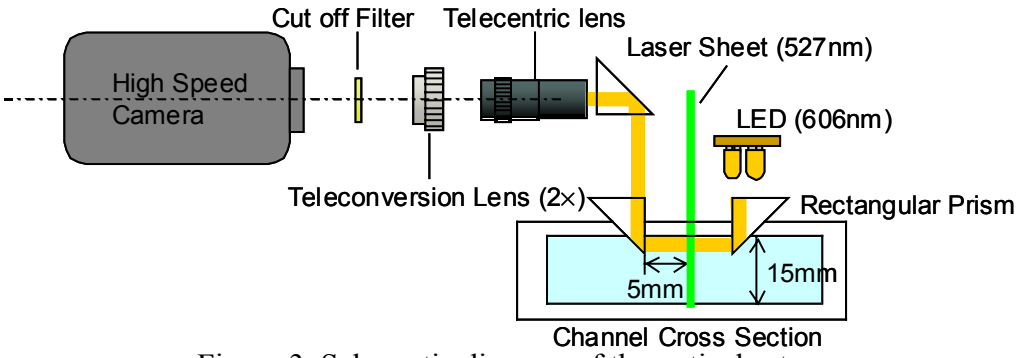

Figure 3. Schematic diagram of the optical setup.

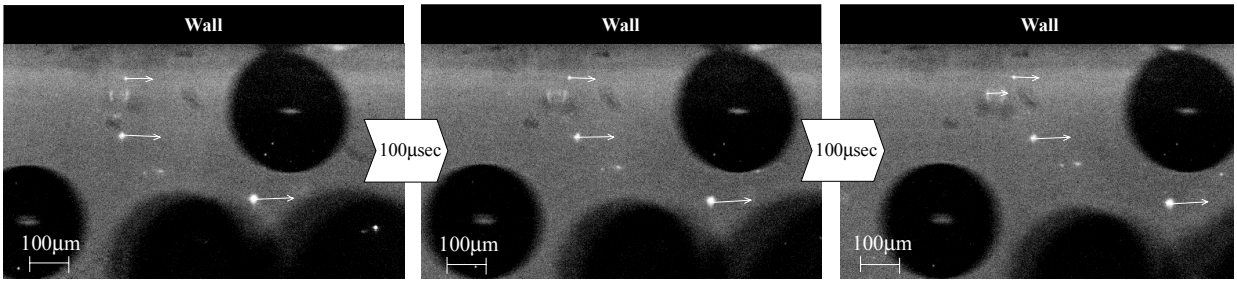

Figure 4. Schematic images of flow field with PTV vector.

3.2 Shear stress sensor

The wall shear stress was measured in the test section using skin friction sensor (S10W, Sankei Engineering) as shown in fig.5. The sensor has a sensing disk, which has a diameter of 10mm and the maximum load of 19.6×10^{-3} N which is corresponding to5010 micro-strain. The sensor was set in the center plane of the test section and mounted flush on the upper wall. The strain gauge connected to a strain amp (Kyowa Dengyo, DPM-713B), and the output signal from the strain amp is sampled by an AD converter. The sampling rate was set at 20Hz. In a static calibration of the shear sensor, it loaded of 5000 micro-strain to the strain amp and measured the output signal.

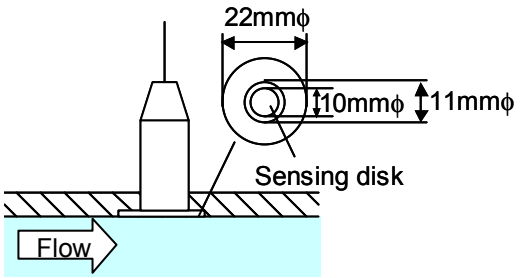

Figure 5. Schematic diagram of shear stress sensor.

4. Results and discussion

4.1 High Magnified telecetric PIV/PTV

4.1.1 Measurements in the single phase flow

The statistic velocity profile was got by averaging of the result of PTV for 50,000 pares of images. Figure 6 shows the dimensionless velocity profiles u^+, which were nondimensionalized by the friction velocity, against y^+. The profile in single phase flow agrees well with the wall function in viscous sub layer and the wall function in inner layer.

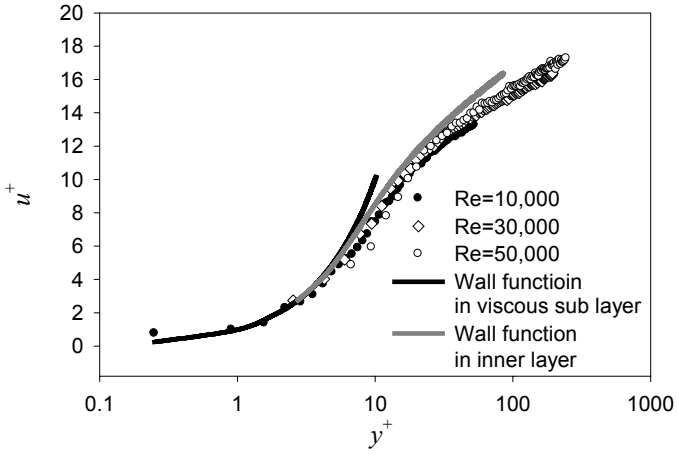

Figure 6. Velocity profile in near wall region.

4.1.2 Measurements in the two phase flow

The example of captured images for the void fraction of 0.04 are show in figure 6, 7 and 8 corresponding to Reynolds number is 10,000, 30,000 and 50,000, respectively.

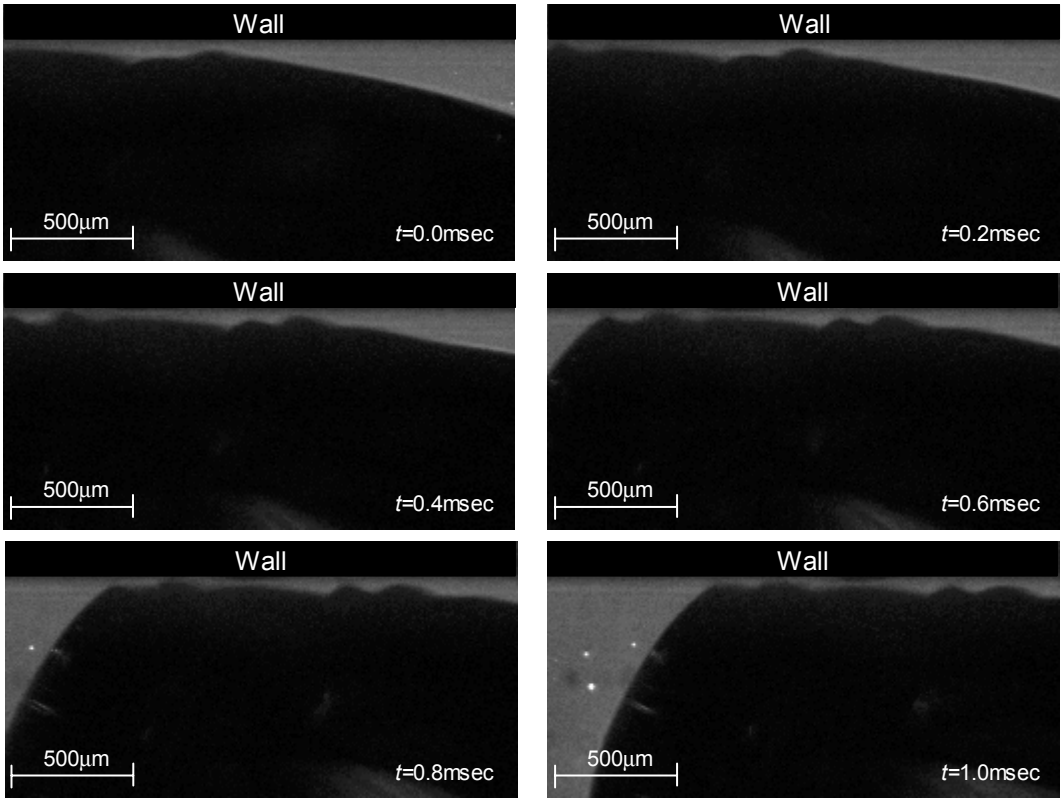

Figure 6. The example of captured image, Re=10,000, α=0.04.

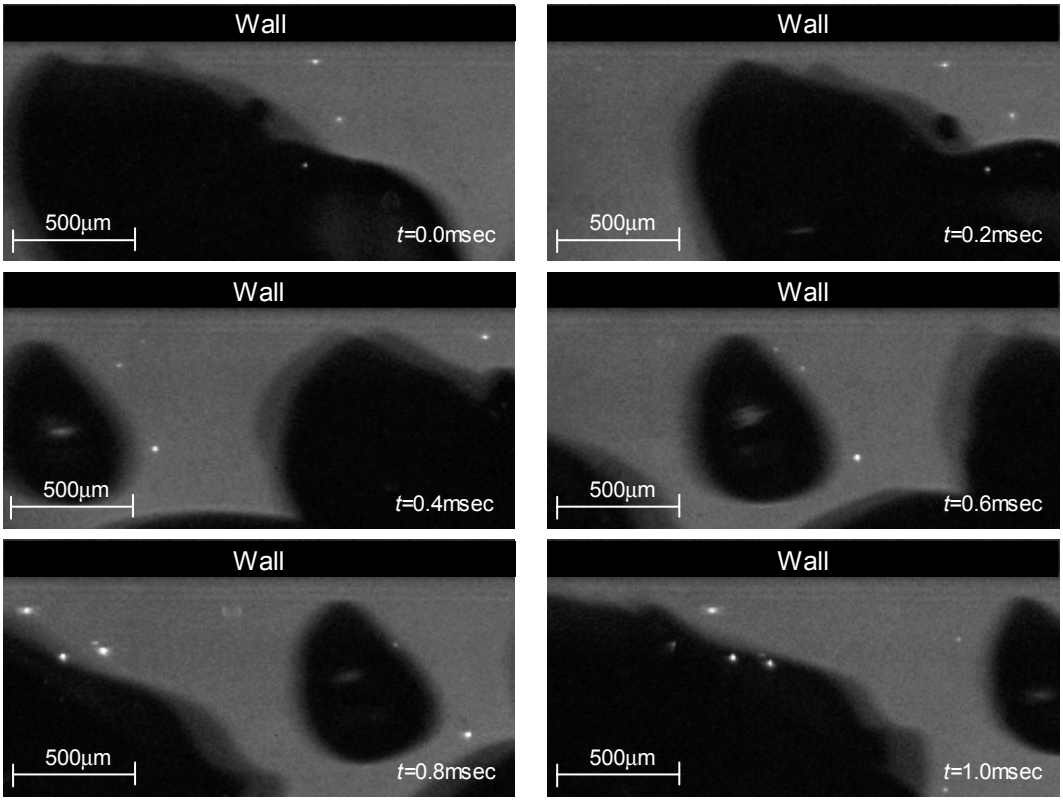

Figure 7. The example of captured image, Re=30,000, α=0.04.

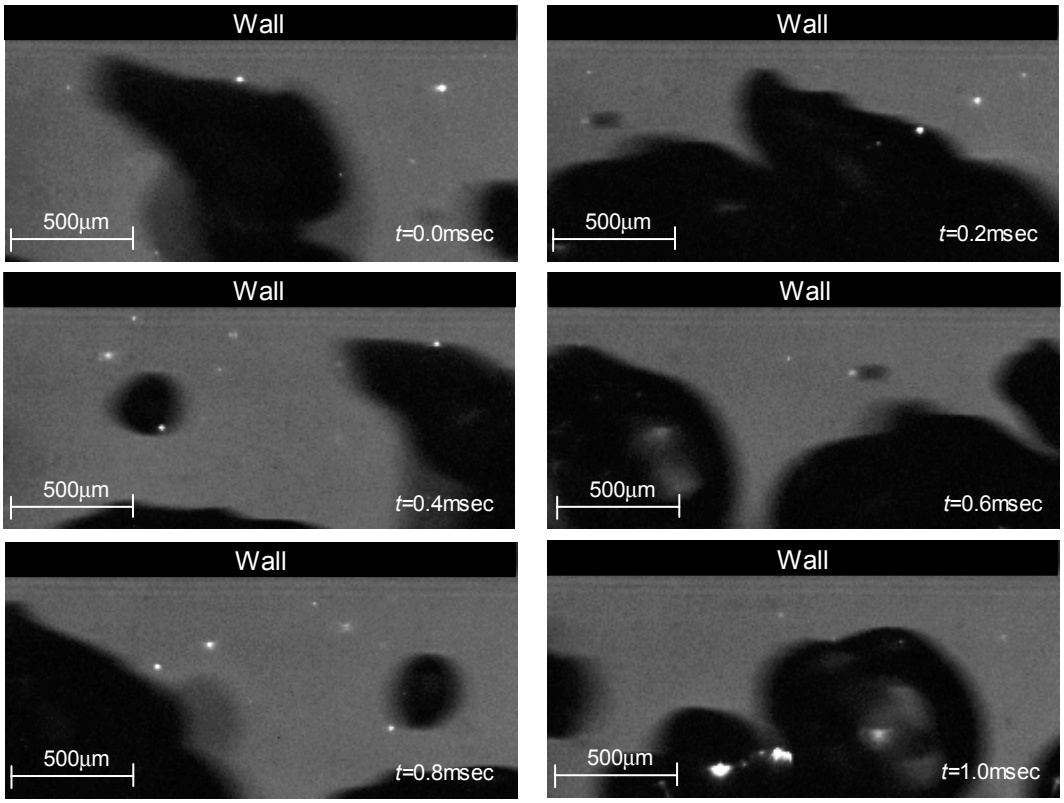

Figure 8. The example of captured image, Re=50,000, α=0.04.

In the images, The black areas, the gray areas and the white spots are corresponding to the gas phase, the liquid phase and the tracer particles, respectively. The ghost of the bubble was given by the unfocused bubble.

The velocity profile and turbulent intensity are shown in Figure 9, 10 and 11.

For Reynolds number is 10,000, it was confirmed that the velocity was increasing with the increase of the void fraction, which is support the results by the shear stress sensor measurements. In particular, it was significant increase of the velocity for the y is 0 to 500μm, and the turbulence intensity was increased in the measurement section. The large bubbles of approximately 5mm in diameter contacted to the wall and accelerated by the flow of outer layer, thus it was changed that the turbulent flow structure near the wall by the injection of air.

The statistics of the velocity and the turbulent intensity in flow direction was reduced by the air injection for Reynolds number of 30,000. The maximum turbulent intensity reduction was approximately 10% for void fraction of 0.04. The bubble diameter was approximately 1mm and below that is small compared with the bubble for Reynolds number of 10,000, which enables to be effective in reducing the wall shear stress. In addition, the bubble's behavior is different as compared to the case of low Reynolds number, which is not creeping on the wall.

In the case of Reynolds number of 50,000, there was no noticeable modification of flow structure by bubble injection. It can be seen that the reason of the ineffectiveness is low local void fraction in near wall region. For high Reynolds number, the inertia force of flow is dominant, and the buoyancy of the bubble weakened. The bubbles diffuse to the broad area, thus the bubble's effect to the wall reduces.

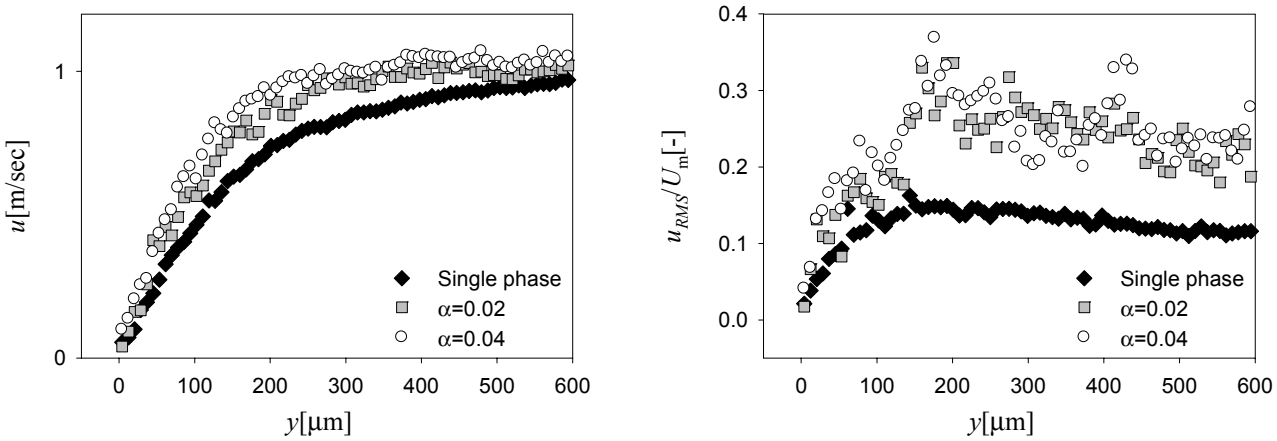

(a) Mean velocity. (b) Turbulence intensity.

Figure 9. Profile of mean velocity and turbulent intensity, Re=10,000.

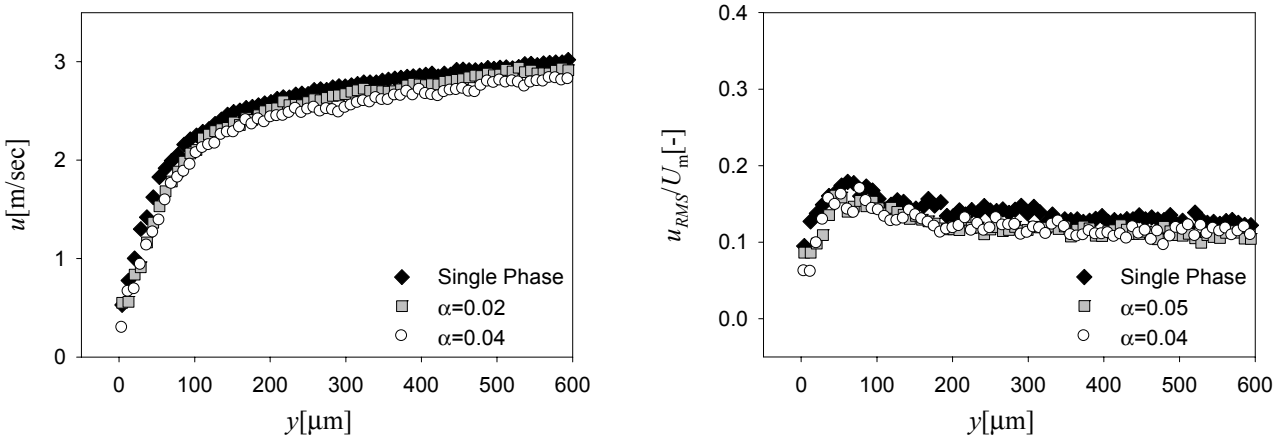

(a) Mean velocity. (b) Turbulence intensity.

Figure 10. Profile of mean velocity and turbulent intensity, Re=30,000.

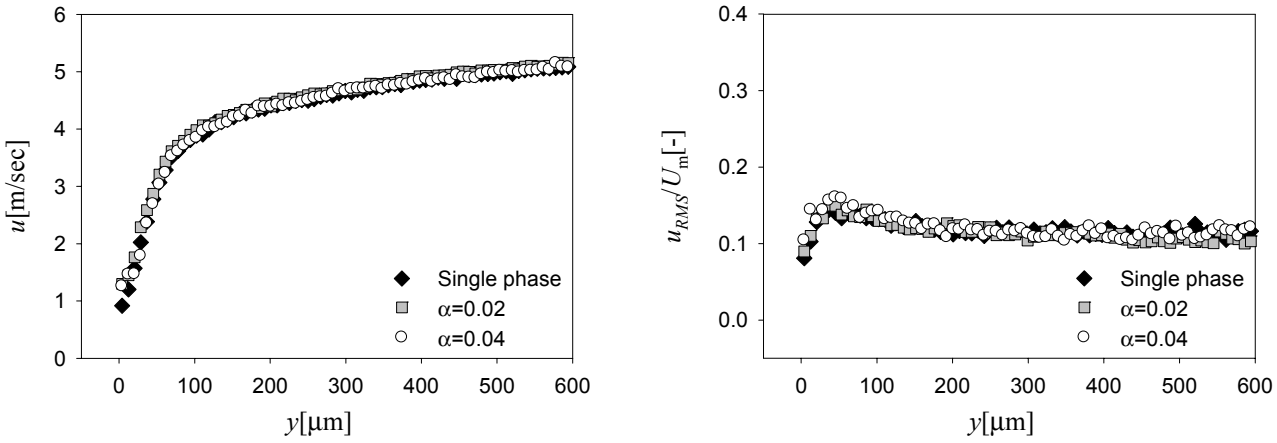

(a) Mean velocity. (b) Turbulence intensity.

Figure 11. Profile of mean velocity and turbulent intensity, Re=50,000.

4.2 Wall shear stress measurement

Figure 12 shows the friction coefficient that measured for Reynolds number is 10,000 to 50,000. The spline curve is an empirical formula obtained by Merkle et al. (1990)

$$\frac{C_f}{C_{f0}} = 0.8e^{-4\alpha} + 0.2 . \qquad (2)$$

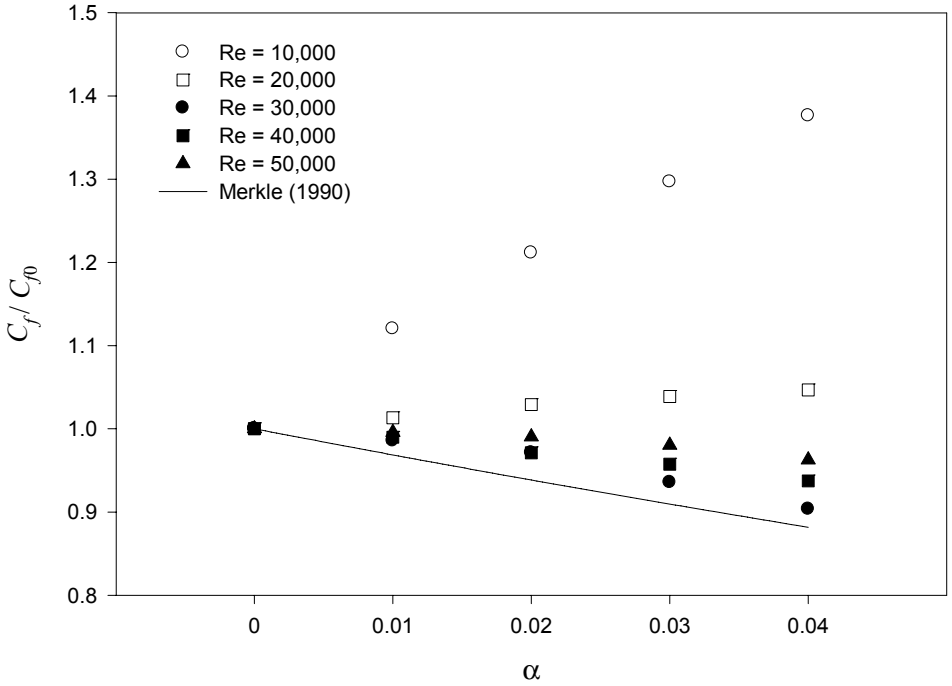

Figure 12. Friction coefficient.

For low Reynolds number of 10,000 and 20,000, the wall shear stress was increasing as the amount of void fraction increased. The maximum friction coefficient increase was approximately 40%. In contrast, the wall shear stress was reducing with increasing of air injection for high Reynolds number of 30,000, 40,000 and 50,000. The maximum skin friction reduction was approximately 10%.

The large bubble of approximately 5mm in diameter for Reynolds number of 10,000 was

creeping on the wall (Figure 6). The bubbles' sizes were decreasing with the velocity increased, because the shear stress on the porous plate increase. It is can be seen that a locally velocity was accelerated between the wall and the bubble when the large bubble creep on the wall, thus the wall shear stress increased with the increase of the void fraction for low Reynolds number.

The drag reduction was more effective in the case of Reynolds number of 30,000 than that of 50,000. It is considered to be caused by a bubble's diffusion by high turbulent flow. Kodama (2000) said that the drag reduction effect decrease with the increasing of a distance between the bubble generator and test section by the measurement of the skin friction. Merkle's empirical equation was given for the distance of 50 – 65mm. In the present study, it can be seen that the distance of 500mm is enough to diffuse the bubbles to an ineffective condition of microbubble drag reduction.

5. Conclusions

The turbulence structure of micobubble drag reduction flow was investigated experimentally using the Highly Magnifying Telecentric PIV/PTV and the shear stress sensor. Under the conditions for Reynolds number ranging from 10,000 to 50,000 and void fraction up to 0.04, the following conclusions are summarized from the present study:

1. It enables to measure the micro flowstructure in near wall region by the Highly Magnifying Telecentric PIV/PTVsystem, and the results indicates that the turbulent flow structure consistent to the results of the wall shear stress measurement.
2. In the case of Reynolds number of 10,000, the large bubbles creep on the wall, thereby the wall shear stress and the turbulent intensity was increasing with the increase of air injection rate.
3. The bubbles reduce the drag force for Reynolds number of 30,000 and over, moreover it was confirmed that the reducing of the mean velocity and the turbulent intensity in near wall region.
4. The drag reduction effect weakens for Reynolds number of 50,000 with little modification of the flow structure. It can be seen the cause that the the turbulent flow diffuses the bubbles to the distant region from the wall.

Acknowledgement

This research was subsidized by the Grant-in-Aid for Scientific Research of Ministry of Education, Culture, Sports, Science and Technology. (No. 17360423)

References

Bogdevich VG; Evees AR; Malyuga AG et al. (1977) GasSaturation Effect on Near-Wall Turbulence Characteristics, 2nd Int. Conf. on Drag Reduction, Cambridge, England, BHRA, pp. 25-37.

Gür Y and Leehey P (1989) A new wall shear stress gauge, Experiments in Fluids, vol. 8, pp. 145-15, 1989.

Fourguette D et al. (2003) Optical Microsensors for Fluid Flow Diagnostics, 41st AIAA Aerospace Sciences Meeting and Exhibit, AIAA-2003-742.

Kato H; Iwashita T; Miyanaga M; Yamaguchi H (1998) Effect of Microbubble Cluster on Turbulent Flow Structure, IUTAM Symp. on Mechanics of Passive and Active Flow Control, Gottingen, Germany, pp. 1-6.

Kitagawa A; Hishida K; Koadama Y (2005) Flow Structure of microbubble-laden turbulent channel flow measured by PIV combined with the shadow image technique, Exp. in Fluids, Vol. 38, pp.466-475.

Kodama Y; Kakugawa A; Takahashi A; Kawashima A (2000) Experimental study on microbubbles and their applicability to ships for skin friction reduction, Int. J. Heat and Fluid Flow, vol. 21, pp. 582-588.

Madavan NK; Deutsch S; Merkle C (1984) Reduction of turbulent skin friction by microbubbles, Phys. Fluids, 27, pp. 356-363.

McCormic ME; Bhattacharyya R (1973) Drag Reduction of a Submersible Hull by Electrolysis, Nav. Eng. J., vol. 85, pp. 11-16.

Merkle C; Deutsch S (1990) Drag Reduction in Liquid Boundary Layers by Gas Injection, Progress in Astronautics and Aeronautics, vol. 123, AIAA, pp 351-412.

Saitoh Y; Hishida K (2004) Optical Measurement of Velocity Gradient in the Near-Wall Region of Microbubble-Laden Turbulent Channel Flow, Pros. 3rd International Symposium on Two-Phase Flow Modeling and Experimentation, Pisa, Italy, 22-24 September 2004, pp.919-926.

Yoshino T; Suzuki Y; Kasagi N; Kamiuten S (2004) Optical Thermal Design of Micro Hot-film Wall Shear Sensor, 689. JSME, vol. 70, pp. 38-45.

Wang ZY (1993) Experimantal study of a wall shear stress sensor based on a porous element, Experiments in Fluids, vol. 14, pp. 153-157.